

Plane-wave DFT-LDA calculation of the electronic structure and absorption spectrum of copper

Andrea Marini, Giovanni Onida, and Rodolfo Del Sole

Istituto Nazionale per la Fisica della Materia, Dipartimento di Fisica dell'Università di Roma "Tor Vergata,"

Via della Ricerca Scientifica, I-00133 Roma, Italy

(Received 18 April 2001; published 22 October 2001)

We present an accurate, first-principles study of the electronic structure and absorption spectrum of bulk copper within density functional theory in the local density approximation, including the study of intraband transitions. We construct norm-conserving pseudopotentials (PP's) including the $3d$ shell (and optionally the underlying $3s$ and $3p$ shells) in the valence and requiring a relatively small plane-wave basis (60 and 140 Ry cutoff, respectively). As a consequence, these PP's are strongly nonlocal, yielding macroscopically wrong results in the absorption spectrum when momentum matrix elements are computed naively. Our results are compared with experimental photoemission, absorption, and electron energy loss data, and suggest nontrivial self-energy effects in the quasiparticle spectrum of Cu.

DOI: 10.1103/PhysRevB.64.195125

PACS number(s): 78.40.Kc, 71.15.Dx, 71.20.-b, 78.20.-e

I. INTRODUCTION

Copper has played for a long time a central role in the elucidation of the electronic structure of solids. It is a relatively inert material, very easy to handle experimentally; its energy dispersion relations (including the spin-orbit interaction for some bands) have been measured with considerable precision; lifetimes of the band states as a function of the distance from Fermi level have been determined; surface states have been analyzed in various parts of the surface Brillouin zone (for a review see Ref. 1). From the theoretical side, the study of noble metals like copper using first-principles methods based on plane-wave and *ab initio* pseudopotentials (PP's) presents some peculiar complication with respect to the case of simple metals or semiconductors. In fact, in addition to metallicity, which implies the use of an accurate sampling of the Brillouin zone in order to describe properly the Fermi surface, one must also keep into account the contribution of d electrons to the bonding and to the valence band structure. This means that, within the PP scheme, d states cannot be frozen into the core part, but must be explicitly included into the valence, yielding a large total number of valence electrons (11 for bulk copper). Unfortunately, a Cu pseudopotential including third-shell states into the valence part is very steep. Hence, when working with a plane-wave basis, the use of a PP of this kind may be computationally prohibitive.

On the other hand, the use of a pseudopotential without explicit treatment of $3d$ electrons has been shown to be unreliable.² Hence, first-principles methods based on plane waves have been used only seldom to treat Cu.² However, methods have been devised for the construction of softer pseudopotentials,³⁻⁶ which make the inclusion of the third shell in the valence more affordable. The price to be paid is that the construction and use of such pseudopotentials, which often display a very strong l nonlocality, is a quite delicate matter. In particular, the choice of a reference component⁷ and the transferability checks must be done with care. These difficulties are more than compensated by the simplicity and elegance of the plane-wave formalism in the subsequent calculations. In the present work, two possible choices for the

Cu pseudopotential are explored, i.e., (a) including $3s$ and $3p$ electrons into the frozen core (a quite standard choice) and (b) including the full third shell in the valence. Fully converged density functional theory and local density approximation (DFT-LDA) calculations are performed at 60 and 140 Ry cutoff, respectively, for cases (a) and (b).

The paper is organized as follows: in Sec. II we give the details of the construction of the pseudopotentials used throughout this work; in Secs. III and IV we present the ground-state properties and band structure, respectively, obtained with the different pseudopotentials; finally, in Sec. V, we compare the theoretical absorption and electron energy loss spectra with the experimental data, including the effects of local fields and intraband transitions.

II. PSEUDOPOTENTIAL GENERATION

The Cu atom has the ground-state electronic configuration $[\text{Ar}]3d^{10}4s^1$ (or $[\text{Ne}]3s^23p^63d^{10}4s^1$). $4s$ and $3d$ eigenvalues are separated, in DFT-LDA, by less than 0.5 eV. It is then quite obvious that freezing all states but the $4s$ one into the atomic core (i.e., to neglect the polarization of the $3d$ electrons) cannot yield a good, transferable pseudopotential. On the other hand, inclusion of the $3d$ electrons in the valence (we call this a “ $3d$ ” pseudopotential) yields a much slower convergence of plane-wave expansions, due to the steepness of the d component of the PP. Unfortunately, the spatial superposition between the $3d$ and $3s$ or $3p$ states is quite large, despite the large (≈ 70 eV) energy separation. Hence, an even more conservative and secure choice for the PP is to include all $3s$, $3p$, and $3d$ electrons into the valence: in fact, $2p$ and $3s$ states are well separated, both spatially and energetically (≈ 800 eV). This latter choice gives rise to a PP which is even harder than the “ $3d$ ” one and which will be referred to as a “ $3s$ ” pseudopotential, yielding 19 valence electrons per atom.

Using the traditional pseudopotential generation scheme proposed by Bachelet, Hamann, and Schlüter⁷ (BHS) yields a PP whose d component converges very slowly in Fourier space, requiring one to work at an energy cutoff of 200 Ry or more. However, PP's which converge at less than 100 Ry can

TABLE I. Cu pseudopotential cutoff radii and reference components. (H) and (TM) stand for the Hamann (Ref. 8) and Troulliers-Martins (Ref. 6) schemes, respectively. All our pseudopotentials are norm conserving in the sense of Bachelet, Hamann, and Schlüter (Ref. 7), and have been produced using a publicly available FORTRAN code (Ref. 28). They are also available in numerical form upon request by electronic mail to: onida@roma2.infn.it

Pseudopotential	r_s [bohr]	r_p [bohr]	r_d [bohr]	Reference l component
“3d”	1.19 (H)	1.19 (H)	2.08 (TM)	s
“3d+NLCC”	1.10 (H)	1.19 (H)	2.08 (TM)	s
“3s”	0.49 (H)	0.60 (H)	1.19 (TM)	p

be constructed by using specially devised schemes as those of Refs. 3–6. We choose to restrict to the class of *norm-conserving* pseudopotentials, in order to avoid the additional numerical complications arising from the charge-state dependence of the PP of Ref. 3. Moreover, our choices in generating the PP are dictated not only by the need of a fast convergence of the PP in Fourier space, but also by that of optimizing the PP accuracy and transferability, a nontrivial task when also $3s$ and $3p$ states are included in the valence. In particular, the Hamann scheme⁸ (which does not try to optimize the Fourier space convergence at all) turned out to yield much more accurate and transferrable norm-conserving PP’s, particularly when the whole third shell is included in the valence.

Hence, we strictly follow the Hamann procedure (described in the Appendix of Ref. 8) whenever it is possible, i.e., in all cases except for the d components. For the latter, we follow the Troullier-Martins⁶ (TM) scheme, which allows us to reduce significantly the number of plane waves requested for convergence without losing too much in transferability. In all other cases (i.e., for the s and p components of both “3s” and “3d” pseudopotentials) we found the Hamann procedure to be more convenient, even at the cost of a slower Fourier space convergence, since the TM one yielded significantly worse results and/or ghost states⁹ when the PP were used in the Kleinman-Bylander (KB) form.¹⁰

Another delicate point is the choice of a reference component, i.e., of a PP angular momentum component which is taken to be valid for every $l \geq 3$. Often, the $l=2$ component is chosen as a reference, simply because this makes calculations easier. This choice is sometimes lacking a physical justification and can be dangerous, as has been shown by some of us in the case of Sn.¹¹ In the present case the $l=2$ reference had to be avoided anyway, since it yielded a much worse transferability than the $l=0$ or $l=1$ choices and sometimes gave rise to ghost states in the KB form.

Several trials and tests with different cutoff radii have been done, in order to optimize the PP transferability without increasing too much the number of plane waves requested for convergence. Transferability tests included both the plot of logarithmic derivatives and the explicit calculation of pseudoatom eigenvalues in some excited electronic configuration (both neutral and positively charged).

Finally, since $3s$ and $3p$ states in the solid preserve their atomic configuration better than $3d$ ones, their explicit inclusion in the valence can sometimes be avoided, by considering only the effects of the nonlinearity of the exchange-

correlation potential.¹² Hence, a third pseudopotential, with frozen $3s$ and $3p$ electrons but including nonlinear core corrections (NLCC), has also been considered and will be referred to as the “3d+NLCC” PP. In the latter, the core charge is represented by the true one for $r \geq 0.5$ bohr and by a Gaussian model charge for $r \leq 0.5$ bohr.

The resulting optimal cutoff radii and reference l components, chosen for our “3d”, “3s”, and “3d+NLCC” pseudopotentials, are given in Table I.

III. GROUND-STATE PROPERTIES

Our first step is a self-consistent ground-state calculation, performed by minimizing the DFT-LDA energy functional with a Car-Parrinello method,¹³ in a standard plane-wave basis. The Ceperley-Alder¹⁴ exchange-correlation energy and potential, as parametrized by Perdew and Zunger,¹⁵ have been used (test calculations with the Hedin-Lundqvist form¹⁶ have also been performed: see below). All our pseudopotentials are used within the fully separable Kleinman-Bylander scheme,¹⁰ after checking that no ghost states were present.⁹ The irreducible wedge of the Brillouin zone (IBZ) was sampled with the use of Monkhorst-Pack (MP) sets¹⁷ of N_k \mathbf{k} points. A very small fictitious electronic temperature (equal to ≈ 10 K) was used in order to accelerate the convergence of the calculated Fermi surface. Convergence with respect to both the \mathbf{k} -point sampling and the kinetic energy cutoff has been checked extensively: Figure 1 and Table II show the results obtained for the “3d” pseudopotential. $E_{cut} = 60$ Ry and $N_k = 28$ appear to give well-converged, satisfactory results, with lattice constant a_0 and bulk modulus B_0 within 1.4% of the experimental values. In the calculation with the NLCC PP, the energy cutoff had to be increased to 100 Ry, in order to describe properly the core charge. The NLCC PP reduces the underestimation of the experimental lattice constant to 0.5%, but they are found to be almost uninfluential on the band structure, as well as on the resulting spectra (see below). Finally, calculations with the “3s” pseudopotential, much deeper than the “3d” one, required an energy cutoff of 140 Ry. Also in this case, the effect on the LDA band structure and spectra in the energetic region of interest are found to be very small (see below).

In summary, as long as only the LDA $4s$ and $3d$ band structure is concerned, the effect of the inclusion of $3s$ and $3p$ in the valence (as well as the use of NLCC) is mainly confined to a change of the equilibrium lattice constant,

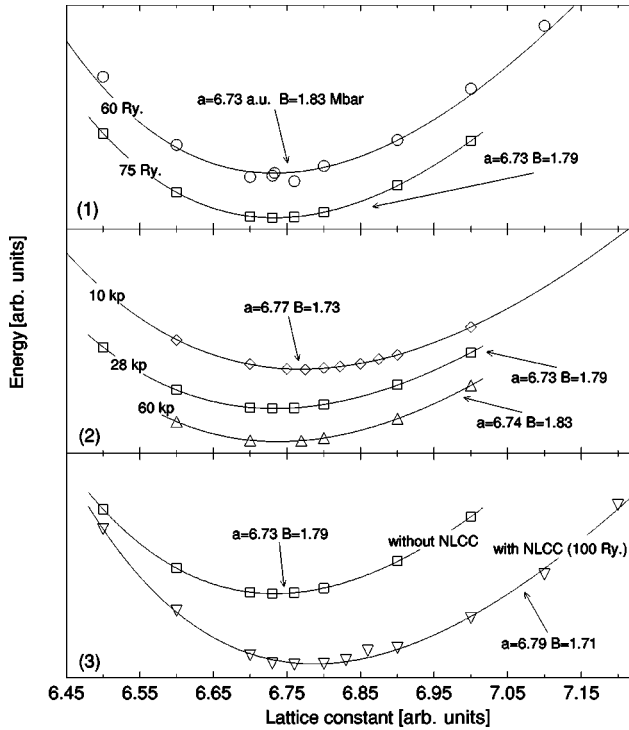


FIG. 1. Calculated total energy vs lattice constant for bulk Cu. Panel (1): effect of the kinetic energy cutoff at fixed number of \mathbf{k} points (28). Panel (2): effect of the IBZ sampling at fixed E_{cut} (75 Ry). Panel (3): effect of nonlinear core corrections (see text). The reported values for the equilibrium lattice constant and bulk modulus have been obtained from Murnaghan fits (solid curves). The experimental values are $a = 6.822$ bohrs and $B = 1.827$ Mbar (Ref. 29).

which induces an indirect effect on the band structure energies.¹⁸

IV. LDA BAND STRUCTURE

Figure 2 summarizes the maximum relative energy differences induced by different computational details on the LDA band structure; the value is taken at the bottom valence in the Γ point (Γ_1) and decreases gradually to zero at the Fermi level.

By changing E_{cut} from 60 Ry to 75 Ry the band structure remains practically identical (changes are less than 0.02 meV). At the 60 Ry cutoff, we compare the band structure calculated with the Ceperley-Alder parametrization of the

TABLE II. Convergence of the calculated ground-state properties of bulk Cu.

PW cutoff (Ry)	N_k	a_0 [bohr]	B_0 [Mbar]
75	10	6.77	1.73
75	28	6.73	1.79
75	60	6.74	1.83
60	28	6.73	1.83
100+NLCC	28	6.79	1.71
Expt.	–	6.82	1.83

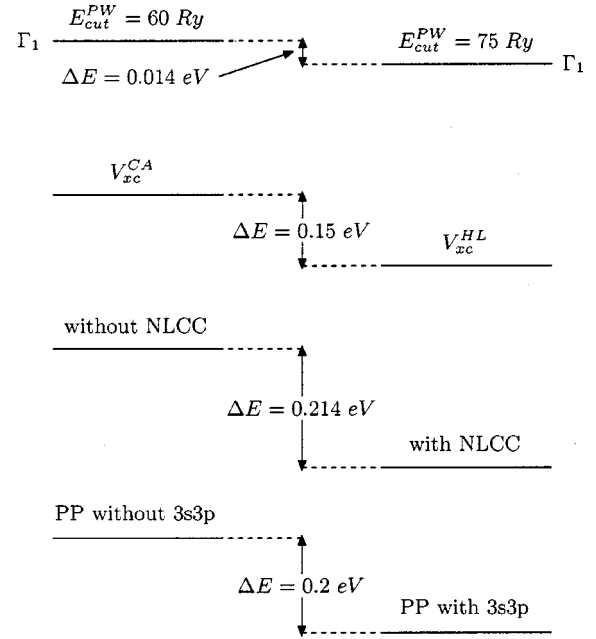


FIG. 2. Summary of the effects of different computational details on the LDA band structure. The energy differences reported are the maximum ones and correspond to the bottom valence at the Γ point (Γ_1). They decrease gradually to zero at the Fermi level.

exchange-correlation potential^{14,15} with that obtained using the Hedin-Lunqvist parametrization,¹⁶ in the latter case we find a maximum energy shift of about 0.15 eV.

The inclusion of NLCC yields, instead, a maximum upward shift of about 0.21 eV with respect to the case without NLCC, mainly due to the change in the equilibrium lattice constant. To study more deeply the effects of core polarization, we also performed a band structure calculation with the “3s” pseudopotential (see Sec. II), where the 3s and 3p core level relaxation is fully included in the self-consistent run. Also in this case the maximum band shift with respect to the “3d” pseudopotential is limited to about 0.2 eV. Hence, our results obtained with the “3d” pseudopotential at $E_{cut} = 60$ Ry and using 28 MP \mathbf{k} points in the determination of the self-consistent charge density can be considered to represent the converged LDA band structure of bulk copper. Theoretical results are compared with the experimental photoemission data in Fig. 3. At difference with the case of semiconductors, the disagreement between theory and experiment is far from being limited to a rigid shift of the Kohn-Sham occupied eigenvalues with respect to the empty ones. In fact, as also summarized in Table III, the widths of the d bands are systematically overestimated, a well-known failure of the LDA when applied to transition and noble metals.¹⁹

V. ABSORPTION SPECTRUM

The absorption spectrum is given by the imaginary part of the macroscopic dielectric function

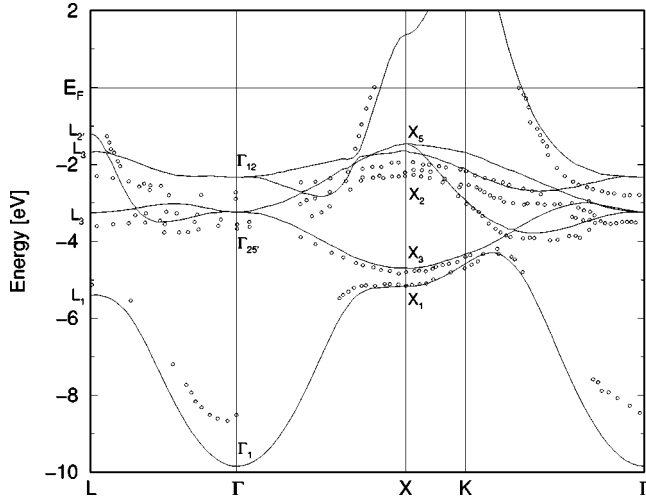


FIG. 3. Bulk copper DFT-LDA band structure (solid line), compared with photoemission data (points) from Ref. 1.

$$\epsilon_M(\omega) = \frac{1}{\epsilon_0^{-1}(\omega)}, \quad (1)$$

where

$$\epsilon_0^{-1}(\omega) = 1 + \lim_{\mathbf{q} \rightarrow 0} \frac{4\pi}{|\mathbf{q}|^2} \chi_{\mathbf{G}=\mathbf{0} \ \mathbf{G}'=\mathbf{0}}(\mathbf{q}, \omega), \quad (2)$$

and $\chi_{\mathbf{G}\mathbf{G}'}(\mathbf{q}, \omega)$ is the reducible polarization, solution of the equation

$$\begin{aligned} \chi_{\mathbf{G}\mathbf{G}'}(\mathbf{q}, \omega) &= \chi_{\mathbf{G}\mathbf{G}'}^0(\mathbf{q}, \omega) + \sum_{\mathbf{G}''} \chi_{\mathbf{G}\mathbf{G}''}^0(\mathbf{q}, \omega) \\ &\times \frac{4\pi}{|\mathbf{q} + \mathbf{G}''|^2} \chi_{\mathbf{G}''\mathbf{G}'}(\mathbf{q}, \omega). \end{aligned} \quad (3)$$

TABLE III. Comparison of Cu bandwidths and energy position with experimental values (Ref. 1) at high-symmetry points. All energies in eV.

		Experiment ^a	Present work
Positions of <i>d</i> bands	Γ_{12}	-2.78	-2.33
	X_5	-2.01	-1.46
	L_3	-2.25	-1.69
Widths of <i>d</i> bands	Γ_{12} - $\Gamma_{25'}$	0.81	0.91
	X_5 - X_3	2.79	3.23
	X_5 - X_1	3.17	3.70
	L_3 - L_3	1.37	1.58
	L_3 - L_1	2.91	3.72
Positions of <i>sp</i> bands	Γ_1	-8.60	-9.85
	$L_{2'}$	-0.85	-1.12
<i>L</i> gap	L_1 - $L_{2'}$	5.20	4.21

^aReference 1.

Neglecting (for the moment) intraband transitions, $\chi_{\mathbf{G}\mathbf{G}'}^0(\mathbf{q}, \omega)$ is given by

$$\begin{aligned} \chi_{\mathbf{G}\mathbf{G}'}^0(\mathbf{q}, \omega) &= \frac{1}{2} \int_{\text{BZ}} \frac{d^3\mathbf{k}}{(2\pi)^3} \sum_{n \neq n'} \langle n' \mathbf{k} - \mathbf{q} | e^{-i(\mathbf{q} + \mathbf{G}) \cdot \mathbf{r}} | n \mathbf{k} \rangle \\ &\times \langle n \mathbf{k} | e^{i(\mathbf{q} + \mathbf{G}') \cdot \mathbf{r}} | n' \mathbf{k} - \mathbf{q} \rangle \mathcal{G}_{he}^0(n, n', \mathbf{k}, \mathbf{q}, \omega), \end{aligned} \quad (4)$$

with

$$\begin{aligned} \mathcal{G}_{he}^0(n, n', \mathbf{k}, \mathbf{q}, \omega) &= f_{n'}(\mathbf{k} - \mathbf{q}) [2 - f_n(\mathbf{k})] \\ &\times \left[\frac{1}{\omega + \epsilon_{n'}(\mathbf{k} - \mathbf{q}) - \epsilon_n(\mathbf{k}) + i\eta} \right. \\ &\left. - \frac{1}{\omega + \epsilon_n(\mathbf{k}) - \epsilon_{n'}(\mathbf{k} - \mathbf{q}) + i\eta} \right], \end{aligned} \quad (5)$$

with $0 \leq f_n(\mathbf{k}) \leq 2$ representing the occupation number summed over spin components. The sums over \mathbf{k} are transformed to integrals over the BZ, and the latter are evaluated by summing over large sets of random points contained in the whole BZ. Fully converged calculations with a small broadening require a very large number of \mathbf{k} points;²⁰ in the present work, the broadening used (and the corresponding number of \mathbf{k} points which was found to be sufficient to ensure convergence) is specified explicitly for each one of the reported spectra.

The simplest approach to the calculation of the absorption spectrum neglects the full inversion of Eq. (3) (i.e., neglects local field effects) and assumes

$$\epsilon_M(\omega) \approx 1 - \lim_{\mathbf{q} \rightarrow 0} \frac{4\pi}{|\mathbf{q}|^2} \chi_{\mathbf{G}=\mathbf{0} \ \mathbf{G}'=\mathbf{0}}(\mathbf{q}, \omega). \quad (6)$$

The $\mathbf{q} \rightarrow \mathbf{0}$ limit for the oscillator strengths appearing in Eq. (4) is calculated in the transverse gauge,²¹ within first-order perturbation theory,²²

$$\begin{aligned} \lim_{\mathbf{q} \rightarrow 0} \langle n' \mathbf{k} - \mathbf{q} | e^{-i\mathbf{q} \cdot \mathbf{r}} | n \mathbf{k} \rangle &= -i\mathbf{q} \cdot \frac{\langle \phi_{n' \mathbf{k} - \mathbf{q}} | [\mathbf{r}, H] | \phi_{n \mathbf{k}} \rangle}{\epsilon_{n'}(\mathbf{k}) - \epsilon_n(\mathbf{k})} \\ &+ O(q^2), \end{aligned} \quad (7)$$

where $\phi_{n\mathbf{k}}(\mathbf{r})$ are the Bloch functions. Due to the nonlocal character of the norm-conserving pseudopotentials, the well-known relation between $[\mathbf{r}, H]$ and the momentum operator,

$$[\mathbf{r}, H] = \mathbf{p}, \quad (8)$$

must be substituted by

$$[\mathbf{r}, H] = \mathbf{p} + [\mathbf{r}, V_{NL}]. \quad (9)$$

The second term on the right-hand side (RHS) of Eq. (9), which in simple metals and in many semiconductors is small (and often neglected in practical calculations), becomes extremely important in the case of copper due to the large nonlocality of the PP. This is demonstrated in Fig. 4 where

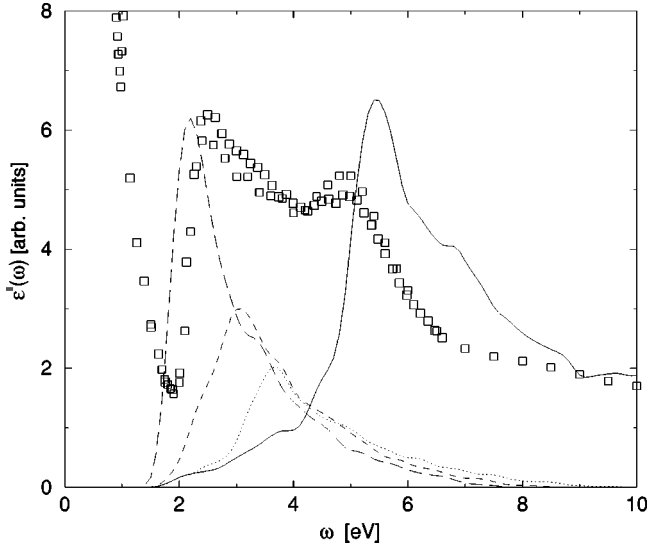


FIG. 4. Solid line: imaginary part of the macroscopic dielectric function of Cu without local field effects and without including the nonlocal pseudopotential commutator [Eq. (9)], compared with experimental data (squares) from Ref. 30. Dot, dashed, and long-dashed lines correspond to the functions defined in Eq. (10) with $n'=3$, $n'=4$, and $n'=5$ respectively. All theoretical curves are computed with $N_k=15386$ and a Gaussian broadening of 0.15 eV (see text).

the imaginary part of ϵ_M is calculated assuming the validity of Eq. (8). The experimental absorption spectrum is severely underestimated between the offset of interband transitions (≈ 1.74 eV) and 5 eV. A better analysis of this behavior can be performed by plotting the quantity

$$\text{Im} \left[\frac{\sum_{\mathbf{k}} \mathcal{G}_{he}^0(n, n', \mathbf{k}, \mathbf{0}, \omega)}{\omega^2} \right], \quad (10)$$

with $n=6$ and $n'=3,4,5$ (see Fig. 4). This quantity is the joint density of states (JDOS) (divided by ω^2) for transitions between the sixth band (sp like) and the third to fifth bands (d like), and corresponds to assuming an oscillator strength equal to one in Eq. (4).

We see that transitions in the energy range of interest (1.8–5.0 eV) exist, but they are strongly suppressed due to the small values of the corresponding matrix elements of \mathbf{p} . Using both terms of Eq. (9), instead, we obtain the spectrum shown in Fig. 5, comparing much better with experiments. The large influence of the nonlocal pseudopotential commutator on $d \rightarrow sp$ optical transitions can be understood by writing explicitly the contribution of the second term of Eq. (9):

$$\begin{aligned} & \langle \phi_{(s/p)\mathbf{k}} | [\mathbf{r}, V_{NL}] | \phi_{(d)\mathbf{k}} \rangle \\ &= \sum_{l=s,p,d} \int \int d\mathbf{r} d\mathbf{r}' \phi_{(s/p)\mathbf{k}}^*(\mathbf{r}) [\mathbf{r} V_{NL}^l(\mathbf{r}, \mathbf{r}') \\ & \quad - V_{NL}^l(\mathbf{r}, \mathbf{r}') \mathbf{r}'] \phi_{(d)\mathbf{k}}(\mathbf{r}'), \end{aligned} \quad (11)$$

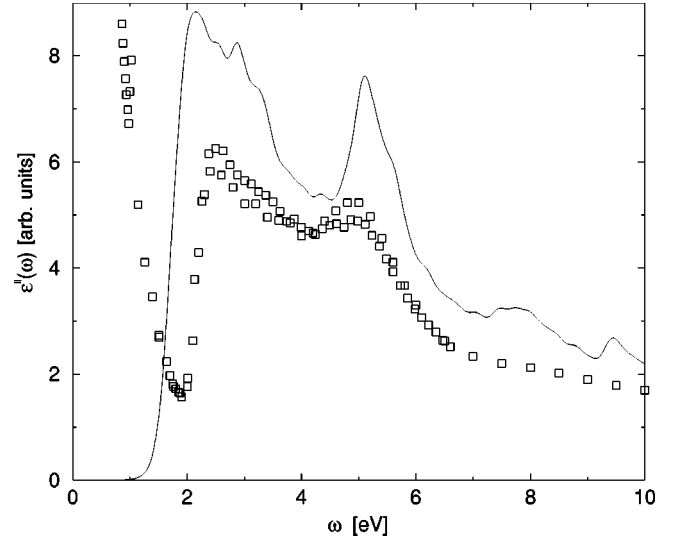


FIG. 5. Solid line: imaginary part of the macroscopic dielectric function of Cu without local field effects and including the nonlocal pseudopotential commutator [Eq. (9)], compared with experimental data (squares) (Ref. 30). N_k and broadening as in Fig. 4.

where $V_{NL}^l(\mathbf{r}, \mathbf{r}')$ is the l -orbital component of the pseudopotential, and $\phi_{(s/p)\mathbf{k}}(\mathbf{r})$, $\phi_{(d)\mathbf{k}}(\mathbf{r})$ are the s/p -like and d -like Bloch functions. Now we can approximate the sum in Eq. (11) with the leading terms, to obtain

$$\begin{aligned} & \langle \phi_{(s/p)\mathbf{k}} | [\mathbf{r}, V_{NL}] | \phi_{(d)\mathbf{k}} \rangle \\ & \approx \int \int d\mathbf{r} d\mathbf{r}' \{ \phi_{(s/p)\mathbf{k}}^*(\mathbf{r}) \mathbf{r} V_{NL}^d(\mathbf{r}, \mathbf{r}') \phi_{(d)\mathbf{k}}(\mathbf{r}') \\ & \quad - \phi_{(s/p)\mathbf{k}}^*(\mathbf{r}) [V_{NL}^s(\mathbf{r}, \mathbf{r}') + V_{NL}^p(\mathbf{r}, \mathbf{r}')] \mathbf{r}' \phi_{(d)\mathbf{k}}(\mathbf{r}') \}. \end{aligned} \quad (12)$$

In the case of copper the d components of the pseudopotential differ from the p component near the origin by about 20 hartrees, and this explains the strong influence on $\epsilon_M''(\omega)$.

Despite the strong improvement of the agreement with experiment obtained in Fig. 5, the theoretical curve exhibits an amplitude overestimation of about 20% with respect to the experimental absorption spectrum.

This drawback must be analyzed taking into account both the *physical approximations* involved in our theoretical approach and the possible *residual errors* due to the PP scheme. Concerning the first ones, the most important point is the neglect of self-energy effects in the band structure calculation and of excitonic effects in the absorption process. Concerning the PP scheme, instead, a possible reason for the overestimation of the spectrum intensity could be related to the use of pseudo wave functions instead of the all-electron ones in Eq. (4). This effect has been studied in atoms by the authors of Ref. 23: they found that PP calculations, even when the second term on the RHS of Eq. (9) is correctly taken into account, can be affected by a small residual error due to the difference between all-electron wave functions and pseudo wave functions *inside the core region*. In the case

TABLE IV. Optical matrix elements for the Cu atom, calculated in the all-electron (AE) scheme and with the pseudopotentials used in the present work. Values are in atomic units.

Optical transitions	AE	“3 <i>d</i> ” PP	“3 <i>s</i> ” PP
4 <i>s</i> →4 <i>p</i>	1.732	1.738	1.713
3 <i>d</i> →4 <i>p</i>	0.406	0.453	0.412

of the Cu atoms, 3*d*→4*p* transitions were found to yield a matrix element which was too large by about 10%.²³

The effect of this overestimation of the 3*d*→4*p* intra-atomic optical matrix elements on the calculated bulk spectrum is, however, not obvious. To clarify this point, we have performed an accurate comparison of the results obtained by using the “3*d*” and “3*s*” pseudopotentials, both in case of the bulk crystal and for the isolated Cu atom. For the latter case, our results are summarized in Table IV: while our “3*d*” pseudopotential gives about the same results as those obtained in Ref. 23, the “3*s*” PP reduces the error in the intra-atomic optical matrix elements to less than 1.5%. However, in the case of the bulk crystal the amplitude of our calculated spectrum does not change appreciably when results obtained with “3*d*” and “3*s*” pseudopotentials are compared (see Fig. 6). This suggests that the overall intensity overestimation cannot be ascribed to the use of PP wave functions in Eq. (4).

The reason for this discrepancy between theory and experiment should hence be searched for within the physical approximations made, such as the neglect of self-energy effects that are currently under investigation and will be the subject of a forthcoming paper.²⁴

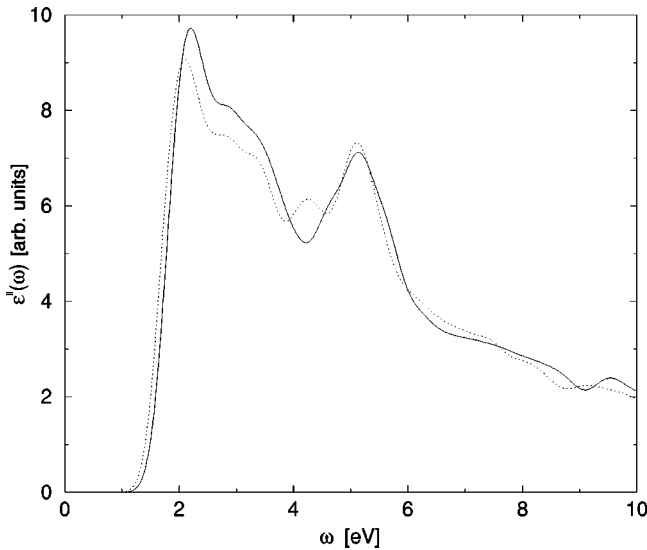


FIG. 6. Effect of the use of a pseudopotential including the 3*s* and 3*p* shells in the valence on the calculated $\epsilon''(\omega)$ for bulk Cu (solid line, “3*d*” PP; dotted line, “3*s*” PP. See text). Due to the large number of plane waves required by the “3*s*” PP, the comparison is done using a small number of \mathbf{k} points and a relatively large Gaussian broadening ($N_k=3000$, $\gamma=0.2$ eV). Local field effects are neglected, and Eq. (9) is used.

A. Intraband transitions

A peculiar characteristic of metals is the intraband contribution to the dielectric function, which, neglecting local field effects, is given by

$$\epsilon'_{intra}(\omega) \equiv 1 - \lim_{\mathbf{q} \rightarrow 0} \left\{ \frac{4\pi}{|\mathbf{q}|^2} \sum_n \int_{BZ} \frac{d^3\mathbf{k}}{(2\pi)^3} [f_n(\mathbf{k}-\mathbf{q}) - f_n(\mathbf{k})] \times \frac{|\langle n\mathbf{k} | e^{i\mathbf{q}\cdot\mathbf{r}} | n\mathbf{k}-\mathbf{q} \rangle|^2}{\omega + \epsilon_n(\mathbf{k}-\mathbf{q}) - \epsilon_n(\mathbf{k})} \right\}, \quad (13)$$

with the n sum restricted only to semioccupied bands. In the case of copper only the sixth band contributes to Eq. (13). Indicating this band with n_F and using the relation

$$\begin{aligned} f_{n_F}(\mathbf{k}-\mathbf{q}) - f_{n_F}(\mathbf{k}) &= [f_{n_F}(\mathbf{k}-\mathbf{q}) - f_{n_F}(\mathbf{k})] \{ \theta[f_{n_F}(\mathbf{k}-\mathbf{q}) - f_{n_F}(\mathbf{k})] \\ &\quad - \theta[f_{n_F}(\mathbf{k}) - f_{n_F}(\mathbf{k}-\mathbf{q})] \}, \end{aligned} \quad (14)$$

time-reversal symmetry allows one to rewrite Eq. (13) as

$$\begin{aligned} \epsilon'_{intra}(\omega) &\equiv 1 - \lim_{\mathbf{q} \rightarrow 0} \left\{ \frac{8\pi}{|\mathbf{q}|^2} \int_{BZ} \frac{d^3\mathbf{k}}{(2\pi)^3} [f_{n_F}(\mathbf{k}-\mathbf{q}) - f_{n_F}(\mathbf{k})] \theta[f_{n_F}(\mathbf{k}-\mathbf{q}) - f_{n_F}(\mathbf{k})] \right. \\ &\quad \left. \times \frac{|\langle n\mathbf{k} | e^{i\mathbf{q}\cdot\mathbf{r}} | n\mathbf{k}-\mathbf{q} \rangle|^2 [\epsilon_{n_F}(\mathbf{k}) - \epsilon_{n_F}(\mathbf{k}-\mathbf{q})]}{\omega^2 - [\epsilon_{n_F}(\mathbf{k}) - \epsilon_{n_F}(\mathbf{k}-\mathbf{q})]^2} \right\}. \end{aligned} \quad (15)$$

In the small- \mathbf{q} limit, Eq. (15) yields the well-known Drude contribution to the dielectric function

$$\epsilon'_{intra}(\omega) \equiv 1 - \frac{\omega_D^2}{\omega^2} + O(q^2), \quad (16)$$

with

$$\begin{aligned} \omega_D^2 &= \lim_{\mathbf{q} \rightarrow 0} \left\{ \frac{8\pi}{|\mathbf{q}|^2} \int_{BZ} \frac{d^3\mathbf{k}}{(2\pi)^3} [f_{n_F}(\mathbf{k}-\mathbf{q}) - f_{n_F}(\mathbf{k})] \theta[f_{n_F}(\mathbf{k}-\mathbf{q}) - f_{n_F}(\mathbf{k})] \right. \\ &\quad \left. \times \frac{|\langle n\mathbf{k} | e^{i\mathbf{q}\cdot\mathbf{r}} | n\mathbf{k}-\mathbf{q} \rangle|^2 [\epsilon_{n_F}(\mathbf{k}) - \epsilon_{n_F}(\mathbf{k}-\mathbf{q})]}{\omega^2} \right\}. \end{aligned} \quad (17)$$

Since the θ function in Eq. (17) limits strongly the region of the BZ that contributes to the integral, the \mathbf{k} -space sampling and the modulus of the chosen \mathbf{q} vector used in the numerical evaluation of Eq. (17) become two critical convergence parameters: for a small $|\mathbf{q}|$ very few \mathbf{k} points will satisfy the condition $[f_{n_F}(\mathbf{k}-\mathbf{q}) - f_{n_F}(\mathbf{k})] \neq 0$. In practice, $|\mathbf{q}|$ must be small enough to reproduce the $\mathbf{q} \rightarrow 0$ limit in Eq. (17), but large enough to allow a suitable number of \mathbf{k} points to contribute to the sum. To obtain a well-converged ω_D^2 we found

TABLE V. Cu Drude plasma frequency and optical mass values obtained using different fictitious electronic temperatures; the experimental value for m_{opt} is 1.35 (Ref. 25).

T_{el} [eV]	Number of intraband transitions	ω_D [eV]	m_{opt}
0.1	14,617	9.39	1.32
0.01	2,456	9.41	1.32
0.001	534	9.25	1.36
0.0001	310	9.28	1.36
0.00001	296	9.27	1.36

it necessary to use $\approx 16\,000$ random \mathbf{k} points in a region of the BZ such that $\epsilon_{n_F}(\mathbf{k})$ is contained within $\epsilon_{Fermi} \pm 0.1$ eV. The value used was $|\mathbf{q}| = 0.005$ a.u. A fictitious electronic temperature was introduced to smear out the Fermi surface, increasing the number of $(\mathbf{k}, \mathbf{k} - \mathbf{q})$ pairs giving nonzero contributions to Eq. (17). In Table V we present our results as a function of the fictitious electronic temperature. The optical mass, defined as

$$m_{opt} = \left(\frac{\omega_c}{\omega_D} \right)^2 \quad \text{with} \quad \omega_c = \sqrt{\frac{4\pi}{\Omega}} = 10.8 \text{ eV}, \quad (18)$$

with Ω being the direct-lattice cell volume, converges to 1.36, a value in good agreement with experiment.²⁵

B. Local field effects

Local field effects are accounted for when the macroscopic dielectric function is computed according to Eqs. (1)–(3), i.e., by explicitly obtaining $\chi_{GG'}(\mathbf{q}, \omega)$ as

$$\chi_{GG'}(\mathbf{q}, \omega) = \chi_{GG'}^0(\mathbf{q}, \omega) \left[1 - \frac{4\pi}{|\mathbf{q} + \mathbf{G}|^2} \chi_{GG'}^0(\mathbf{q}, \omega) \right]^{-1}. \quad (19)$$

We divide explicitly $\chi_{GG'}^0(\mathbf{q}, \omega)$ into intraband and interband contributions:

$$\chi_{GG'}^0(\mathbf{q}, \omega) = \chi_{GG'}^{inter}(\mathbf{q}, \omega) + \chi_{GG'}^{intra}(\mathbf{q}, \omega), \quad (20)$$

where the interband part is given by Eq. (4), while for the intraband contribution we have to evaluate

$$\begin{aligned} \chi_{GG'}^{intra}(\mathbf{q}, \omega) &= \frac{1}{2} \int_{BZ} \frac{d^3\mathbf{k}}{(2\pi)^3} \langle n_F \mathbf{k} - \mathbf{q} | e^{-i(\mathbf{q} + \mathbf{G}) \cdot \mathbf{r}} | n_F \mathbf{k} \rangle \\ &\quad \times \langle n_F \mathbf{k} | e^{i(\mathbf{q} + \mathbf{G}') \cdot \mathbf{r}'} | n_F \mathbf{k} - \mathbf{q} \rangle \\ &\quad \times \mathcal{G}_{he}^0(n_F, n_F, \mathbf{k}, \mathbf{q}, \omega), \end{aligned} \quad (21)$$

with $\mathcal{G}_{he}^0(n, n', \mathbf{k}, \mathbf{q}, \omega)$ defined in Eq. (5). For $G, G' \neq 0$ the oscillator strength is calculated using fast Fourier transforms (FFT's),

$$\langle n\mathbf{k} - \mathbf{q} | e^{-i(\mathbf{q} + \mathbf{G}) \cdot \mathbf{r}} | n'\mathbf{k} \rangle = \langle u_{n\mathbf{k}} | e^{-i\mathbf{G} \cdot \mathbf{r}} | u_{n'\mathbf{k}} \rangle + O(q), \quad (22)$$

while for the $G = G' = 0$ element of χ^{inter} we use Eq. (7).

The method presented in Sec. V A for the calculation of ω_D could, in principle, be extended to $\chi_{GG'}^{intra}(\mathbf{q}, \omega)$. Unfortunately the explicit calculation of χ^{intra} for all the $(\mathbf{G}, \mathbf{G}')$ pairs is computationally prohibitive, due to the large number of \mathbf{k} points required to reach convergence. To overcome these difficulties, we have evaluated Eq. (21) on a limited number of \mathbf{k} points (a MP grid of 110 points in the irreducible wedge). $\mathcal{G}_{he}^0(n_F, n_F, \mathbf{k}, \mathbf{q}, \omega)$ is different from zero only for \mathbf{k} very close to the Fermi surface (which, in the grid, coincides with one particular point \mathbf{k}_F) where $f_{n_F}(\mathbf{k} - \mathbf{q}) [2 - f_{n_F}(\mathbf{k})] \neq 0$. The oscillator strengths can be considered to be almost constant in the vicinity of the Fermi surface. The same ansatz cannot be applied to $\mathcal{G}_{he}^0(n_F, n_F, \mathbf{k}, \mathbf{q}, \omega)$; however, we can use the property that near the Fermi surface the metallic band dispersion of copper is well approximated by a free-metal one and make the following assumption for $\chi_{GG'}^{intra}(\mathbf{q}, \omega)$:

$$\begin{aligned} \chi_{GG'}^{intra}(\mathbf{q}, \omega) &\approx \frac{1}{N_s} \left[\sum_{\mathbf{R}} \langle n_F \mathbf{Rk}_F - \mathbf{q} | e^{-i(\mathbf{q} + \mathbf{G}) \cdot \mathbf{r}} | n_F \mathbf{Rk}_F \rangle \right. \\ &\quad \left. \times \langle n_F \mathbf{Rk}_F | e^{i(\mathbf{q} + \mathbf{G}') \cdot \mathbf{r}'} | n_F \mathbf{Rk}_F - \mathbf{q} \rangle \right] \pi_0(\mathbf{q}, \omega), \end{aligned} \quad (23)$$

where \mathbf{R} is one of the N_s symmetry operations not in the point group of \mathbf{k}_F . Here $\pi_0(\mathbf{q}, \omega)$ is the noninteracting polarization calculated for a jellium model²⁶ with a density n_{el} yielding a classic plasma frequency $\omega_p = \sqrt{4\pi n_{el}} = 9.27$ eV, corresponding to the value of ω_D calculated in Sec. V A:

$$\begin{aligned} \pi_0(\mathbf{q}, \omega) &= -\frac{1}{2\pi^2 |\mathbf{q}|} \int_0^{k_F^{j_{el}} |\mathbf{q}|} x dx \left(\frac{1}{\omega - k_F^{j_{el}} |\mathbf{q}| + i\eta} \right. \\ &\quad \left. - \frac{1}{\omega - k_F^{j_{el}} |\mathbf{q}| - i\eta} \right), \end{aligned} \quad (24)$$

where

$$x = \frac{\omega}{k_F^{j_{el}} |\mathbf{q}|} \quad (25)$$

and

$$k_F^{j_{el}} = (r \pi^2 n_{el})^{1/3}. \quad (26)$$

In Fig. 7 we compare our results for $\epsilon''(\omega)$ with and without local field effects (LFE's). The differences are small, consistently with the fact that, as expected, no large LFE's are present in a metal. However, local field effects are more important in electron energy loss spectroscopy (EELS), as shown in Fig. 8: in the high-energy region the full inversion of the $\chi_{GG'}(\mathbf{q}, \omega)$ matrix corrects an overestimation of the intensity. The inclusion of intraband transitions, on the other hand, turns out to be necessary not only to describe correctly the behavior of ϵ'' at low frequencies, but also to improve the agreement of the calculated $\epsilon^{-1}(\omega)$ with the experimental EELS data (Fig. 8).

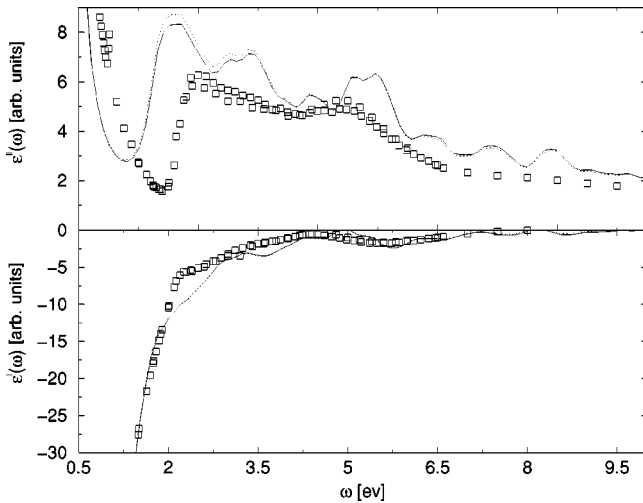


FIG. 7. Real and imaginary parts of $\varepsilon_M(\omega)$ for bulk Cu with (solid line) and without (dotted line) inclusion of local field effects, compared with experimental data (squares) from Ref. 30. Theoretical spectra are computed with $N_k=110$ (in the irreducible wedge of the BZ) and a Lorentzian broadening of 0.4 eV (see text).

VI. CONCLUSIONS

Several conclusions can be drawn from the presented results. First, we have shown that fully converged DFT-LDA calculations for bulk copper using plane waves can be performed without requiring an exceedingly large basis set, by using soft norm-conserving pseudopotentials including the $3d$ electrons in the valence.

The strong nonlocality implied by such pseudopotentials reflects itself in a very large contribution of the commutator between the PP and the position operator in the calculation of the matrix elements entering the dielectric function.

Similar calculations including also the $3s$ and $3p$ shells in the valence are also feasible using plane waves, but show very little difference in the band structure and in the optical matrix elements not directly involving those shells.

At difference with the case of simple semiconductors, the disagreement between the LDA theoretical band structure and the experimental one cannot be corrected by a rigid shift of the Kohn-Sham eigenvalues: this suggests the importance of many-body effects in the quasiparticle spectrum of Cu. These effects should be taken into account through a calculation including self-energy contributions.²⁴ By contrast, the

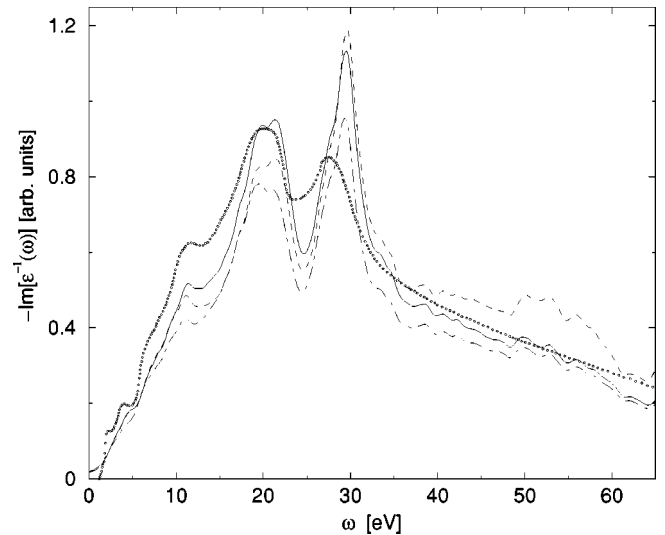


FIG. 8. Imaginary part of the inverse macroscopic dielectric function of Cu including local field effects and the Drude contribution (solid line). Dashed line: results without local field effects. Long-short dashes: with local field effects, but without the Drude contribution. All theoretical spectra are computed with the same N_k of Fig. 7 but with a Lorentzian broadening of 0.9 eV. Points are the EELS data from Ref. 30.

computed optical mass, which involves only intraband transitions at the Fermi energy, is in very good agreement with the experimental data. Also the theoretical absorption spectrum, where only LDA eigenvalues within a few eV around the Fermi energy are important, displays a quite satisfactory agreement with the experimental one. The overall overestimation of about 20% in the amplitude of the main peaks cannot be attributed to the effect of wave function pseudization *inside* the core region and should be ascribed to the neglect of self-energy (and excitonic) effects. Finally, local field effects on the macroscopic dielectric function turn out to be negligible, with or without inclusion of the Drude term.

ACKNOWLEDGMENTS

This work has been supported by the INFN PRA project “1MESS” and by the EU through the NANOPHASE Research Training Network (Contract No. HPRN-CT-2000-00167). We thank L. Reining and A. Rubio for useful discussions. We are grateful to S. Goedecker for providing us an efficient code for fast Fourier transforms.²⁷

¹R. Courths and S. Hüfner, Phys. Rep. **112**, 53 (1984).

²I. Campillo, A. Rubio, and J. M. Pitarke, Phys. Rev. B **59**, 12 188 (1999).

³D. Vanderbilt, Phys. Rev. B **41**, 7892 (1990).

⁴A. M. Rappe, K. M. Rabe, E. Kaxiras, and J. D. Joannopoulos, Phys. Rev. B **41**, 1227 (1990).

⁵E. L. Shirley, D. C. Allan, R. M. Martin, and J. D. Joannopoulos, Phys. Rev. B **40**, 3652 (1989).

⁶N. Troullier and J. L. Martins, Phys. Rev. B **43**, 1993 (1991).

⁷G. Bachelet, D. R. Hamann, and M. Schlüter, Phys. Rev. B **26**, 4199 (1982).

⁸D. R. Hamann, Phys. Rev. B **40**, 2980 (1989).

⁹X. Gonze, P. Käckell, and M. Scheffler, Phys. Rev. B **41**, 12 264 (1990).

¹⁰L. Kleinman and D. M. Bylander, Phys. Rev. Lett. **48**, 1425 (1982).

¹¹M. Meyer, G. Onida, M. Palumbo, and L. Reining, Phys. Rev. B **64**, 045119 (2001).

- ¹²S. G. Louie, S. Froyen, and M. L. Cohen, Phys. Rev. B **26**, 1738 (1982).
- ¹³R. Car and M. Parrinello, Phys. Rev. Lett. **55**, 2471 (1985).
- ¹⁴D. M. Ceperley and B. I. Alder, Phys. Rev. Lett. **45**, 566 (1980).
- ¹⁵J. P. Perdew and A. Zunger, Phys. Rev. B **23**, 5048 (1981).
- ¹⁶L. Hedin and B. I. Lundqvist, J. Phys. C **4**, 2064 (1971).
- ¹⁷H. J. Monkhorst and J. D. Pack, Phys. Rev. B **13**, 5188 (1976).
- ¹⁸However, as long as we are interested in bare LDA results, the overall effect on the $3d$ - $4s$ band structure and on the absorption spectrum is small and, *a posteriori*, we can simply use our “ $3d$ ” PP.
- ¹⁹R. O. Jones and O. Gunnarsson, Rev. Mod. Phys. **61**, 689 (1989).
- ²⁰S. Albrecht, L. Reining, G. Onida, V. Olevano, and R. Del Sole, Phys. Rev. Lett. **83**, 3971 (1999).
- ²¹R. Del Sole and R. Girlanda, Phys. Rev. B **48**, 11 789 (1993).
- ²²M. S. Hybertsen and S. G. Louie, Phys. Rev. B **35**, 5585 (1987).
- ²³J. Read and R. J. Needs, Phys. Rev. B **44**, 13 071 (1991).
- ²⁴A. Marini, R. Del Sole, and G. Onida (unpublished).
- ²⁵H. Ehrenreich and H. R. Philipp, Phys. Rev. **128**, 1622 (1962).
- ²⁶R. D. Mattuck, *A Guide to Feynman Diagrams in the Many-Body Problem* (McGraw-Hill, New York, 1976), pp. 196–200.
- ²⁷S. Goedecker, Comput. Phys. Commun. **76**, 294 (1993); SIAM J. Sci. Comput. (USA) **18**, 1605 (1997).
- ²⁸M. Bockstedte, A. Kley, J. Neugebauer, and M. Scheffler, Comput. Phys. Commun. **107**, 187 (1997).
- ²⁹R. W. G. Wyckoff, *Crystal Structure*, 2nd ed. (Interscience, New York, 1976).
- ³⁰E. D. Palik, *Handbook of Optical Constants of Solids* (Academic Press, New York, 1985).